DISTORTION ANALYSIS OF A WELDED CORNER STIFFENING FRAME CONSIDERING MANUFACTURING RESTRAINING CONDITIONS

M. Stoschka[1], T. Loose[2], Z. Barsoum[3]

[1] Chair of Mechanical Engineering, Dept. Product Engineering, Montanuniversät Leoben, 8700 Leoben, Franz-Josef-Strasse 18, Austria; phone ++43 / 3842 402 - 1455; mailto:michael.stoschka@unileoben.ac.at
[2] Ingenieurbüro Tobias Loose, 75045 Wössingen, Germany
[3] KTH Royal Institute of Technology, Dept. of Aeronautical &Vehicle Engineering, Division of Lightweight Structures, 10044 Stockholm, Sweden

Abstract

This paper studies the applicability of thermo-mechanical coupled weld simulations (*Sysweld*®, *simufact.welding*®) vs. simplified methods (*Weldis*®) based on the inherent strain formulation. A procedure is introduced to derive characteristic inherent strain values from thermo-mechanical coupled simulation runs. Experimental work focusses on a T-joint made of medium-strength structural steel *S355* to validate the numerical distortion results. Further on, different restraining conditions are studied and a numerical framework is built-up to cover this influence on distortion. Finally, the developed inherent strain procedure is applied to a more complex corner stiffening frame in which the aspect of boundary condition modelling is examplified.

Keywords: Transversal joint, Distortion engineering, Inherent strain, Weld simulation.

1 Introduction

The precedent distortion engineering of welded steel frames at design stage is important to be competitive in manufacturing of such structures. Besides the employees expertise in complex interactions of welded structures during welding, numerical engineering tools offer the possibility to determine the distortion at design stage. In the recent years, significant improvements in three-dimensional simulation of welded joints were achieved, both in terms of numerical methods and availability of high-power-computing. An example of an experimentally validated T-joint is depicted in [1], and a three-dimensional finite-element model of a multi-pass joint assembly is shown in [2], demonstrating the general applicability for more complex parts and components. Structural thermo-mechanical coupled weld simulation is beneficial to determine the effect of welding sequence [3] at the design stage and therefore provides a tool to minimize the total costs of a welded structure. Although the thermal elastic-plastic simulation is a very powerful tool to calculate distortion and residual stress distributions after the welding process, its applicability is limited to comparably small parts and assemblies due to computing time limitations.

A comprehensive overview of the numerical capabilities to simulate the welding process is given in [4]. Decoupling the thermal solution from the mechanical part and application of several simplification hypotheses can reduce the computational time [5, 6], but the transient elastic-plastic mechanical solution still defines the major task to solve [7]. There are numerous contributors affecting distortion in welded structures; especially, heat-source input definition, thermal and mechanical material properties, phase transformations, contact conditions as well as root gap and misalignments, weld sequence, tacking and restraining conditions influence the results in a complex way. The basic interaction process between distortion and residual stress due to welding is described in [8]. Key factors for simulation are the appropriate models for heat input, material behaviour and contact definition. The inherent deformation of a welded structure is strongly influenced by change of the plastic deformation from room temperature to melting temperature; but additional factors such as the ‘restrained’ movement of each part due to clamping or tacking [9, 10] have to be considered. Especially the latter has a minor effect on residual stress distribution but might play a significant role on the welding-induced distortion.

Whereas 3D models are able to predict the distortion and stress distribution in an accurate way even for flexible and thin structures, 2D models should be used preferably for thick-walled parts and multi-pass joints [11]. The residual stress distribution of 2D models is mostly satisfying, but the evaluated distortions may be incorrect especially in case of thin plates. In the following, characteristic factors in regard to welding simulation are briefly discussed.

- The influence of restraint condition on the residual stress distribution and distortion for single- and multi-pass welds is studied in [12-15]. External restraints reduce the amount of angular bending distortion induced by the transverse plastic strain distribution. The clamping condition of the welded structure can be quantitatively described by the intensity of restraint [16]. Beside the stiffness of the clamping tool, the release time plays a decisive factor for the amount of distortion [17].
- The influence of mesh density for three-dimensional weld simulation is investigated in [18, 19]. To achieve accurate bending results in case of transversal joints, an outward coarsening of the mesh should be avoided.
- The metallurgical solid-state phase transformation in steels has to be taken into account if the welding process of high-strength steels containing characteristic amounts of bainitic or martensitic microstructure is simulated [20-22]. Further on, the effect of the applied plasticity theory for welded joints is a current research topic [23, 24].
- Investigations in [25] showed that not only the maximum heat input, but in particular the transient shape of the molten zone has a major effect on the final distortion of the part. The correctness of thermal analysis is therefore most important to obtain accurate welding-induced distortions of steel structures.
- A study of inherent welding deformations using an interactive substructure method was done in [26, 27]. The main benefit of this method is a reduction of computational time by negligible decrease of accuracy [28]. In [29], the method of rapid-dumping is presented which also significantly lowers the computational time of three-dimensional weld simulation models.

An alternative and very efficient method to predict distortions of welded large scale structures represents the inherent strain method [30]. The prerequisite to apply this method is the knowledge of the initial deformations for a specific joint. These values can be derived from structural weld simulation or experimental measurements. Welding distortion calculation of plate structures by means of elastic finite element method is presented in [31, 32]. The distortion of the welded parts is evaluated based on inherent strains, whereas the assembly process as well as initial gaps can be taken into account by use of interface elements in the joined components. The theory of effective and non-effective inherent strains is explained in a general form in [33]. The total strain ε in the vicinity of a weld can be subdivided into elastic strain ε^e, plastic strain ε^p, thermal strain ε^T, creep strain ε^C and strain due to phase transformations ε^{tr}. The deformation and stress distribution of a welded joint depends on the total strain reduced by the elastic part, leading to the definition of the inherent strain ε^*.

$$\varepsilon - \varepsilon^e = \varepsilon^p + \varepsilon^T + \varepsilon^C + \varepsilon^{tr} = \varepsilon^* \qquad (1)$$

The interactions between inherent strain, stress, and deformation are depicted in [34] for thin-plates. The inherent strains can be integrated over the cross-section normal to the welding line. This leads to the four main fundamental inherent distortion components, namely longitudinal δ^*_L and transverse δ^*_T shrinkage as well as longitudinal θ^*_L and transverse θ^*_T bending angles.

$$\delta^*_L = \frac{1}{h}\iint \varepsilon^*_X \, dydz \qquad (2)$$

$$\delta^*_T = \frac{1}{h}\iint \varepsilon^*_Y \, dxdz \qquad (3)$$

$$\theta^*_L = \frac{1}{I_{YY}}\iint \varepsilon^*_X \, dydz \qquad (4)$$

$$\theta^*_T = \frac{1}{I_{XX}}\iint \varepsilon^*_Y \, dxdz \qquad (5)$$

The welding direction is aligned to the x-axis of the coordinate system; the y-axis marks the transversal direction and subsequently defines the plane of the base plate. The z-axis characterizes displacements normal to the base plate, e.g. its deformation values assign the bending behaviour of the subsequent investigated transverse joints. This nomenclature is maintained for data evaluation throughout all transversal joint investigations, even though local coordinate systems in the finite element models have different definitions. To get the inherent deformations per element, the inherent strains must be integrated over the thickness of the plate *h* for the plain shrinkage; in case of bending the second moment of inertia I_{XX}, and I_{YY} respectively, have to be considered in the equation.

The elastic finite element calculation based on inherent strains enables an investigation of twisting and buckling behaviour of thin-plate stiffened structures in a time-efficient manner [35, 36]. In this context, the inverse analysis defines a method to (back-calculate) the inherent strains from the previously evaluated distortion field [37]. Another semi-empirical approach uses the (eigenstrain) reconstruction method to predict the residual stress field based on neutron diffraction measurements [38]. If the inherent strain field is applied as a trigonometric function over the plastic zone it is possible to predict a well matching weld-induced stress field [39]. This also improves the stability regarding the residual stress calculation.

Summing up, three-dimensional thermo-mechanical coupled weld simulation is preferable used for simple joints due to computational time and costs. Simplified methods based on the inherent strain offer a powerful method to assess the inherent deformation after welding. In this paper, the commercially available software suites *Sysweld*® and *simufact.welding*®, both capable of transient thermo-mechanical welding simulation including phase transformation, are used to build up reference simulation models focussing on transversal joints with plate thicknesses of eight and twelve millimetres and varying clamping conditions. The evaluated results are compared to a simplified inherent strain approach using the analytical tool *Weldis*® [40]. In addition, the application of an inverse analysis for the investigated T-joint, based on the inherent shrinkage results of the three-dimensional structural weld simulation, is depicted further on.

2 Experimental work

A transversal joint with a plate thickness of *8 mm* made of *S355* structural steel is used as characteristic specimen to investigate the distortion behaviour. Each seam is welded in a single run, an intermediate cooling time is observed between welding of first and second seam. Each pass is started in the same direction, meaning that starting and ending point are identical. The web plate is tacked at both ends to the base plate. By application of the gas-metal-arc-welding process parameters in Table 1, a nominal throat thickness of *a = 4 mm* could be achieved for both fillet welds.

Table 1 – Welding parameters of T-joint with *8 mm* plate thickness

Voltage *U* [V]	Current *I* [A]	Weld position	Energy input per unit length *Q* [J/mm]	Welding speed *v* [mm/s]
30	*390*	*PB*	*877*	*13.3*

The investigated T-joint possesses a girth width of *300 mm*, a web-plate height of *150 mm* and a total axial length of *300 mm*. Both the experimental measurements and the numerically computed distortion are evaluated at the mid-section of the joint referencing to an axial distance of *150 mm*.

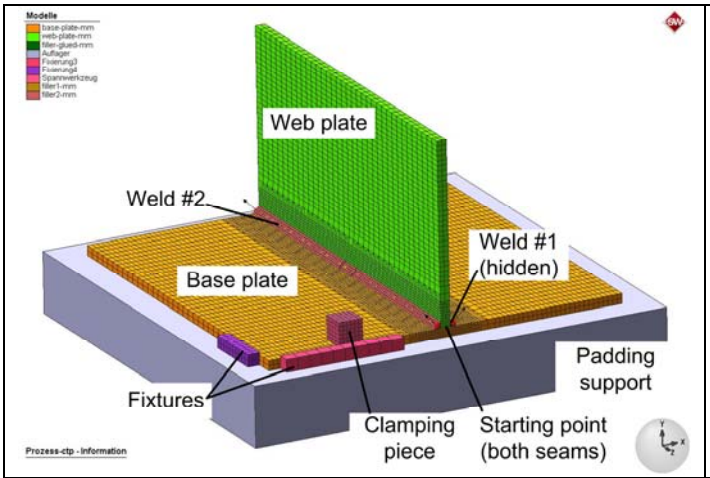

a) Numerical model including clamping conditions

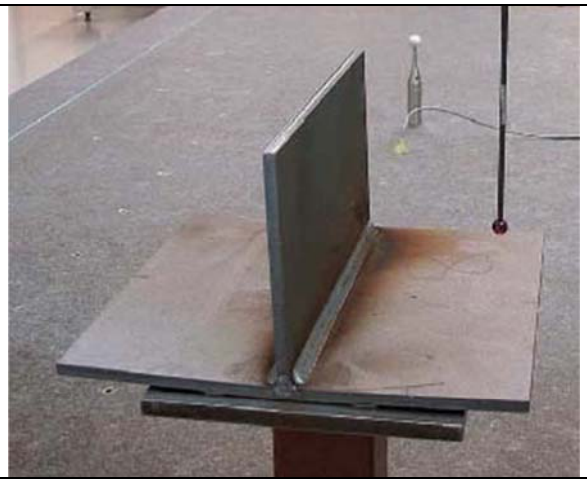

b) Inherent deformation after welding

Fig. 2.1 Investigated T-joint specimen

The manufacturing sequence of the welded joint is depicted in Table 2. The intermediate cooling time of about *6 min* provides a cool-down of the first seam down to about *50 °C*. The thoroughly solidified seam increases the local stiffness of the joint during welding of the second seam. The inherent deformation is evaluated at an end time of *2,000 s*, (facilitating) room temperature within the whole joined part.

Table 2 – Weld sequence of T-joint with *8 mm* plate thickness

Task	Start time [s]	End time [s]
Welding of first seam	*0.0*	*22.5*
Intermediate cooling	*22.5*	*400.0*
Welding of second seam	*400.0*	*422.5*
Final cool-down	*422.5*	*2,000.0*

As shown in Fig. 2.1a, the specimen is fixed to the support plate with a clamping piece applying an initial normal force of *500 N* to the base plate to avoid rigid body motion during welding. The inherent deformation of the unclamped T-joint is shown in Fig. 2.1b. The distorted shape of the base and web plate was scanned using a measurement table. Several T-joint specimens were manufactured (leading to an inherent deformation of about *7.5 mm)* evaluated at the free specimen edge opposite to the clamping point.

3 Computational work

Two independent models of the *8 mm* T-joint were built-up using the simulation suites *Sysweld*® and *simufact.welding*®. The *S355* material database of each program was used for each model postulating an initial ferritic microstructure. Boundary constraints and the weld sequence were applied as defined by the experiments. It has to be mentioned that both codes show distinct differences in representing the contact behaviour between parts. In *Sysweld*®, the contact of the base plate to the padding support is defined by individual contact elements per node. As *simufact.welding*® is based on the *MSC.Marc*® solver, it has the built-in ability to solve the contact between parts automatically via a body-to-body contact definition. Both program suites handle the not-yet-deposited material as quiet elements with significantly reduced mechanical properties, *Sysweld*® uses a stiffness value of *1,000 MPa* and in *simufact.welding*® thousandth of the young modulus is implemented. Both codes take the transient phase transformation into account leading to a dominant bainitic microstructure of the filler metal. The heat-input is defined as a double-ellipsoid model [41]. Fig. 3.1 depicts the transient temperature field for both models during welding of the second seam. A welding heat efficiency of $\eta = 0.85$ for the GMAW-process is considered in the process definition.

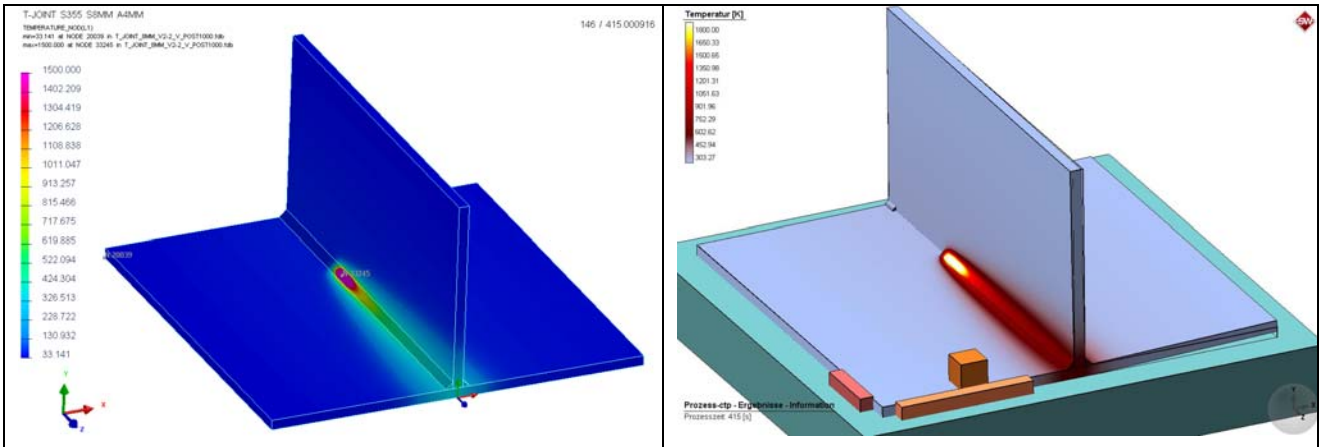

a) Transient temperature field using *Sysweld*® | **b) Temperature result using *simufact.welding*®**

Fig. 3.1 Temperature distribution by numerical weld simulation at $t = 415$ s

The inherent deformation of the ‘unclamped’ T-joint is shown in Fig. 3.2. Both models exhibit a final distortion of about *7.5 mm* at the centre of the free edge which matches the experimental investigations.

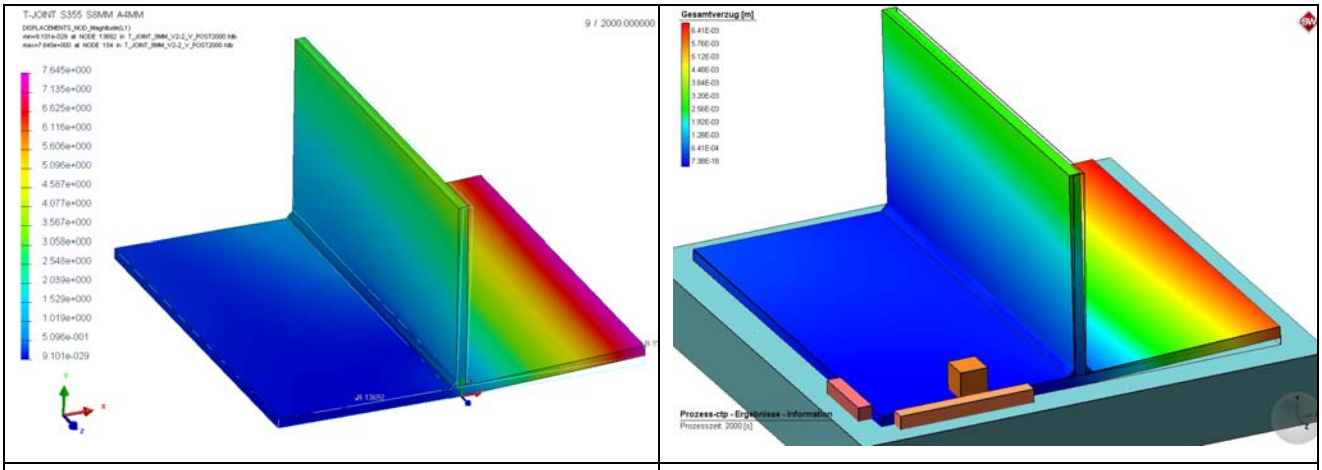

a) Shrinkage after welding using *Sysweld* ® | **b) Shrinkage after welding using *simufact.welding* ®**

Fig. 3.2 Inherent deformation by numerical weld simulation at *t = 2,000 s*

The comparison of the residual stress states in Fig. 3.3 exhibits slight disagreements in the vicinity of the weld seam. This can be explained by small differences in the *S355* material database of each program suite. In *simufact.welding* ®, a slightly more compressive stress field is superimposed at the filler metal boundary due to an increased amount of martensitic solid-state transformation. This reduces the stresses in the heat-affective zone. As the work focuses on the distortion engineering of such joints, this minor difference in residual stress state is neglected.

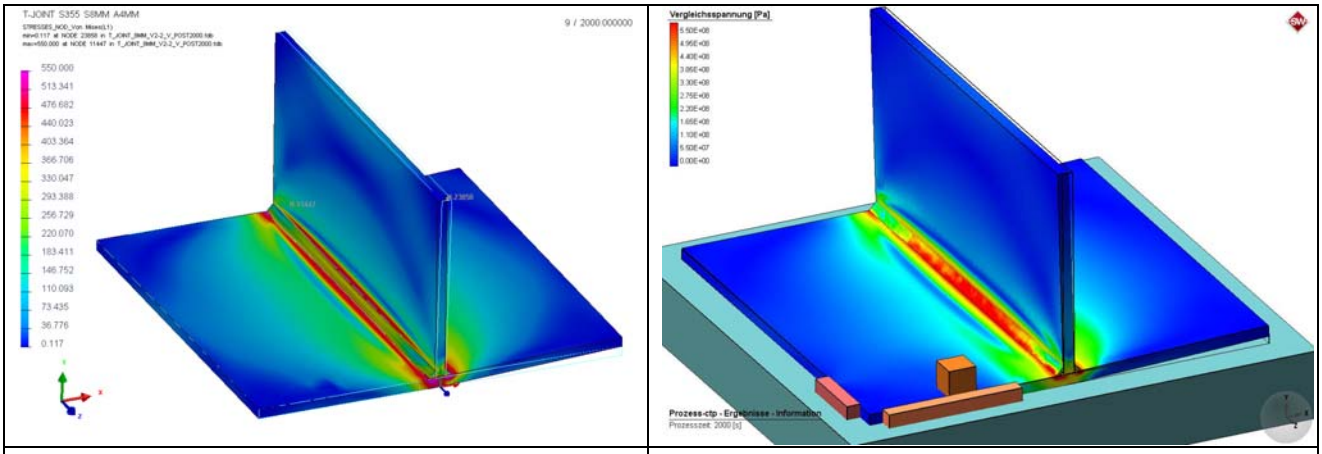

a) Stress result after welding using *Sysweld* ® | **b) Stress result after welding using *simufact.welding* ®**

Fig. 3.3 Equivalent von-Mises stress distribution by numerical weld simulation at *t = 2,000 s*

The experimentally determined inherent deformation validates the predicted numerical distortion results of both software suites. Hence, *Sysweld* ® and *simufact.welding* ® are further on used as *3D*-simulation tools to calculate the deformation of transversal joints with different clamping conditions and varying welding parameters.

3.1 Simplified method based on inherent strain

The four main parameters for the inherent deformation are longitudinal shrinkage, longitudinal bending, transversal shrinkage and transversal bending. The bending moment M_b^* can be expressed as normal distance z^* of the shrinkage force F^* to the neutral axis of the plate. If the local coordinate system is placed into the neutral axis of the plate, the strain distribution in the top/bottom surface can be expressed as the sum of strain caused by shrinkage force and bending moment.

$$\varepsilon_{sum}^* = \frac{F^*}{EA} \pm \frac{M_b^*}{EW_b} \qquad (6)$$

For an element with a rectangular cross section of thickness *z* and length *l*, the strain in the top, middle, and bottom layer can be defined as follows. The mid layer is located in the neutral axis of the plate section.

$$\varepsilon^*_{sum,top} = \iint \varepsilon^* \left(1 + z^* \frac{6}{z}\right) dl\, dz \qquad (7)$$

$$\varepsilon^*_{sum,middle} = \iint \varepsilon^*\, dl\, dz \qquad (8)$$

$$\varepsilon^*_{sum,bottom} = \iint \varepsilon^* \left(1 - z^* \frac{6}{z}\right) dl\, dz \qquad (9)$$

To obtain the inherent strains, several procedures can be applied. First, the inherent strains can be evaluated based on the distribution of the plastic strain by three-dimensional structural weld simulation. Second, the inherent strains can be calculated using the analytical tool *Weldis*®. Third, the inherent strains can be assessed by inverse analysis of a deformed T-joint based on measurements or simulation results.

3.1.1 Evaluation based on thermo-mechanical coupled weld simulation

The dominant transversal inherent deformation is based on the distribution of the transversal plastic strain. Fig. 3.4a depicts the course of the transversal plastic strain at mid cross-section of the T-joint at the top and bottom surface of the base plate. The second seam exhibits a somewhat higher plastic strain which can be explained by the fact that in the case of welding the second seam, the stiffness of the part is already increased due to the deposited filler metal of the first joint.
The stress distribution in transverse and longitudinal direction at top and bottom surface of the base plate is shown in Fig. 3.4b. As the T-joint can bend in transversal direction without additional restraining, the stresses in the longitudinal direction σ_{xx} are most dominant. Outside the heat-affected-zone, the transversal stress equals to zero due to the unhindered bending distortion of the unclamped transversal joint.

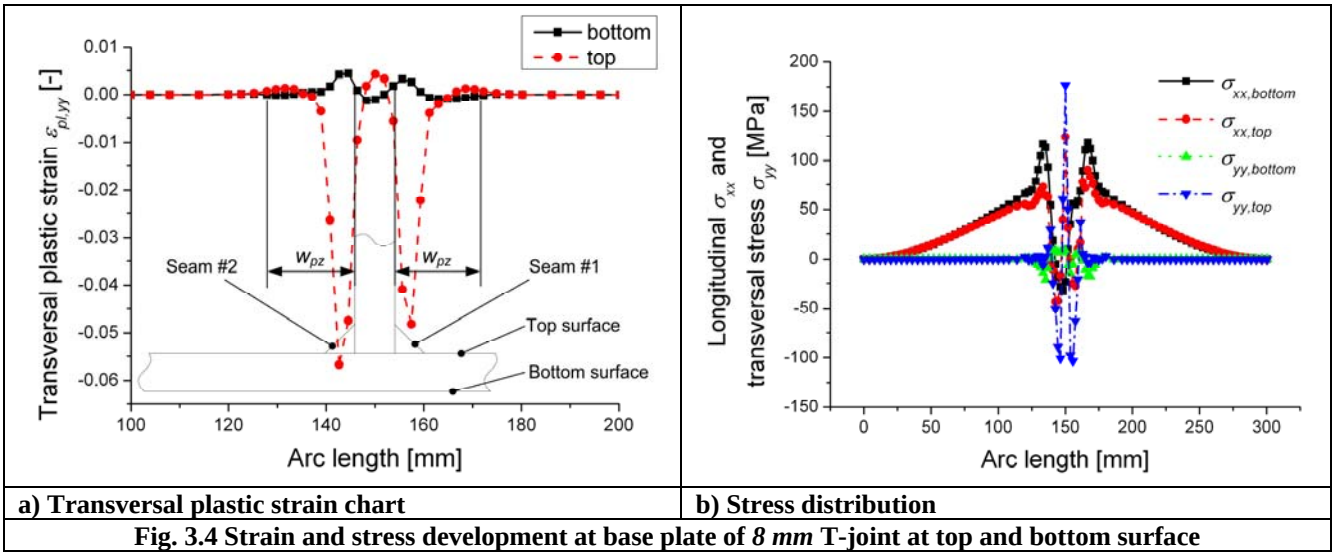

a) Transversal plastic strain chart | **b) Stress distribution**

Fig. 3.4 Strain and stress development at base plate of *8 mm* T-joint at top and bottom surface

Based on the transversal plastic strain course at the top layer of the welding process simulated transversal joint, the width of the plastic zone w_{pz} can be determined using a cut-off limit of *0.05 %*. Subsequently, mean values for the plastic transversal strain are accessible by averaging the values of the plastic strain $\varepsilon_{pl,yy}$ over the width of the plastic zone. Based on these average values $\varepsilon^{avg}_{pl,yy,top}$ and $\varepsilon^{avg}_{pl,yy,bottom}$,, the transverse inherent strain ε^*_{yy} and the offset z^*_{yy} can be calculated. Finally, the bending behaviour of the investigated transversal joint is characterized by the product of inherent strain range between top and bottom layer $\Delta\varepsilon^*_{yy}$ and the width of the plastic zone w_{pz}. This value is further on used for comparison of the inherent distortion between different clamping conditions and geometries. Table 3 sums up the evaluated properties based on the three-dimensional thermo-mechanical coupled weld simulation using *Sysweld*®.

Table 3 – Evaluated inherent properties for T-joint with *8 mm* plate thickness

w_{PZ} [mm]	$\varepsilon^{avg}_{pl,yy,top}$ [-]	$\varepsilon^{avg}_{pl,yybottom}$ [-]	ε^*_{yy} [-]	z^*_{yy} [mm]	$\Delta\varepsilon^*_{yy}\, w_{pz}$ [mm]
16.0	*-0.01207*	*0.00037*	*-0.00585*	*1.42*	*0.199*

Longitudinal shrinkage is based on the longitudinal tensile shrinkage force acting on a small area resembling a tendon. After welding and final cool-down, compressive residual stresses develop in the adjacent plate

area to satisfy the equilibrium condition with the tendon force. These residual compressive stresses can lead to buckling of thin-walled structures after cooling. The shrinkage in longitudinal direction is a function of the ratio between weld cross-section and profile of the surrounding part which resists the thermal expansion of the metal in the heat-affected-zone [42]. In [36], an updated equation for the tendon force is presented based on the net heat-input per unit-length of the welded joint.

$$F_{tendon} = -0.235 Q \eta \qquad [F_{tendon}] = kN, [Q] = \frac{J}{mm} \qquad (10)$$

The longitudinal inherent strain can be calculated from the tendon force if a constant distribution over the plastic zone of the joint is assumed. This leads to an inherent strain value of $\varepsilon^*_{xx} = 0.00326$. Finally, minor longitudinal bending occurs due to the mismatch of the centre position of the heat-affected tendon cross-section compared to the neutral axis of the whole T-joint.

3.1.2 Application of the analytical tool *Weldis*®

Beside the sketched method to determine the inherent strains based on three-dimensional structural weld simulation, the analytical tool *Weldis*® can be used for calculation. Main input parameters are the geometric cross-section, choice of material database and weld manufacturing dependent properties such as net heat-input per unit length, weld velocity, and wire diameter. Output parameters are the width of the plastic zone and the four parameters describing the inherent strain for subsequent elastic finite element simulation.
In regard to the bending behaviour of the web-plate, the second seam counteracts the transient distortion due to welding of the first seam. A parametric study revealed that the counteracting effect of welding the first seam, intermediate cool-down and finally welding of the second seam can be taken into account by considering only one third of the nominal girth bending value for the web-plate inherent strain.

Table 4 – Inherent strains for T-joint with *8 mm* plate thickness by *Weldis*®

w_{PZ} [mm]	ε^*_{xx} [-]	z^*_{xx} [mm]	ε^*_{yy} [-]	z^*_{yy} [mm]	$\Delta\varepsilon^*_{yy} w_{pz}$ [mm]
15.1	-0.00255	0.48	-0.01796	0.73	0.215

This leads to a vertical deflection of the base plate edge of $u_z = 3.99$ *mm*, which is in agreement to the measured value. Fig. 3.5 depicts the results of the finite-element-analysis using the inherent strains calculated with the analytical tool *Weldis*®.
To calculate the inherent deformation based on pre-defined inherent strains, it is only necessary to run an elastic finite element analysis and include the inherent strains as initial state conditions. The finite element suite *Ansys*® supports, since release thirteen, the direct input of elemental strains in the input deck without the additional need of implementing subroutines. The linear-elastic simulation of the shell-model is solved in two steps. First, the layer-dependent inherent strains act as initial conditions in the model, whereas all nodes are fixed in this initial step. By solving this linear step, the nodal reaction forces are calculated by the programme. In the subsequent non-linear load step, the boundary conditions of all nodes are released and only the centre node is fixed to avoid rigid body motion. This boundary condition is equal to the ‘unclamped’ transversal joint previously evaluated in measurement and three-dimensional structural weld simulation.

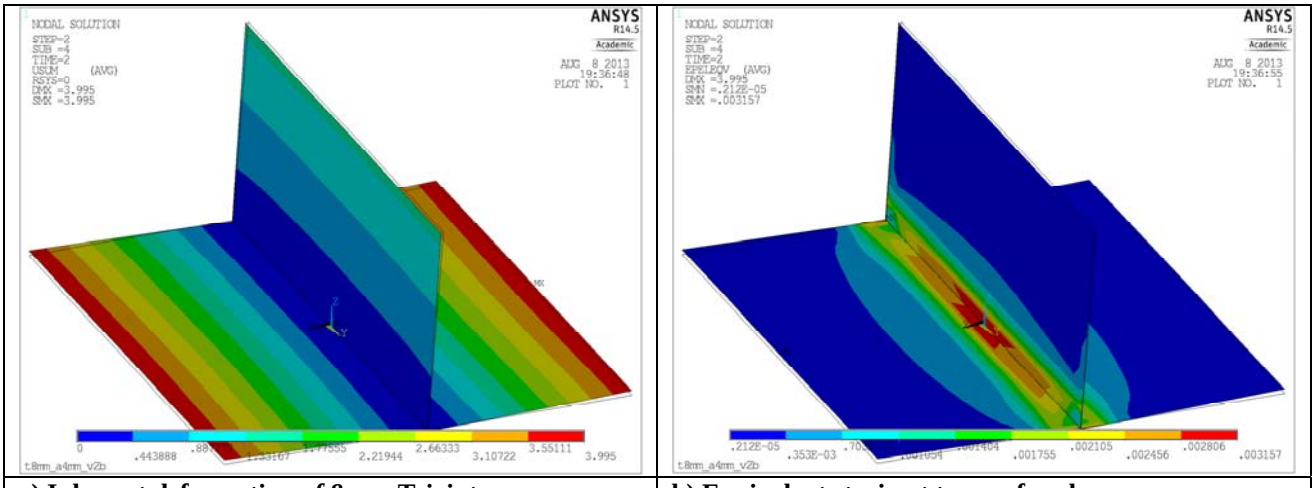

a) Inherent deformation *of 8 mm* T-joint | **b) Equivalent strain at top surface layer**

Fig. 3.5 Results of elastic-finite element analysis using inherent strains calculated by *Weldis*®

3.1.3 Evaluation of inherent strains by inverse analysis

As introduced in [37], the inherent strains can be calculated based on inherent deformation at characteristic points. Fifteen equally spaced points were chosen for evaluation of the distortion dependent value of the four inherent strains. The position of these characteristic evaluation points is shown in Fig. 3.6a. Firstly, the width of the plastic zone was fixed to a value of $w_{pz} = 18.5\ mm$. Secondly, the four inherent strain parameters were randomly calculated and sorted in monotonic order. The inherent strains in longitudinal and transversal direction were varied in ten steps, whereas the two offset values were distributed in five steps to reflect the different bending behaviour. This lead to two and a half thousand linear-elastic simulation runs to gain deformation results for the chosen field of parameters.
For the investigated unclamped transversal joint, the longitudinal strain is generally lower than the transversal strain. In addition, the transversal bending behaviour is more pronounced than the longitudinal one. The four parameters were therefore randomly distributed within reasonable limits; Table 5 lists the field of input values. The expected amount of transversal bending, evaluated as product of transversal strain range and width of plastic zone $\Delta\varepsilon^{*}_{yy}\, w_{pz}$, spans up to $0.945\ mm$.

Table 5 – Inherent strain parameter field for inverse analysis of *8 mm* T-joint

ε^{*}_{xx} [-]	z^{*}_{xx} [mm]	ε^{*}_{yy} [-]	z^{*}_{yy} [mm]
-0.0015	0.101	-0.0076	0.002
-0.0029	0.387	-0.0131	0.420
-0.0036	0.602	-0.0152	0.599
-0.0048	0.675	-0.0170	0.601
-0.0052	0.781	-0.0183	1.166
-0.0054		-0.0203	
-0.0056		-0.0214	
-0.0063		-0.0230	
-0.0088		-0.0255	
-0.0098		-0.0292	

The non-linear data fitting capability of *MatLab®´s* optimization toolbox was used to solve this non-linear problem. Within about hundred iterations, the norm of residuals dropped to a value of less than one millimetre for the fifteen three-dimensional evaluated points. As the number of input parameters is limited, the residual norm can not be reduced further on. This numerical technique of solving the inverse analysis by a parametric study of input parameters, although time consuming, was necessary because the *Ansys®* solver and the optimisation toolbox were accessible only at different workstations. For future work, a direct coupling is scheduled between the optimisation toolbox and the linear-elastic solver by modification of the *Ansys®* input deck directly within a *MatLab®* function. This will reduce the norm of residuals further, but the currently achieved inherent strain result in Table 6 already proves the applicability of the method.

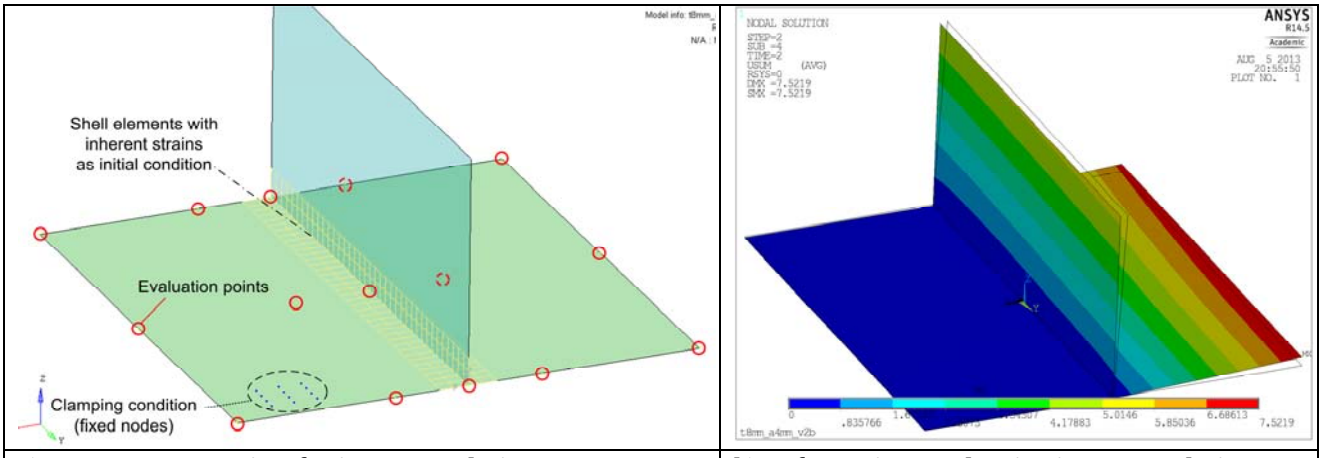

a) Measurements points for inverse analysis | **b) Deformation result using inverse analysis**

Fig. 3.6 Evaluation points and inherent deformation result for inverse analysis

The deformation result of each parametric run was evaluated in agreement to the clamping condition of the experiments. The evaluated mid cross-section inherent deformation value of $u_z = 7.35\ mm$ matches the previous results.

Table 6 – Inherent strains for T-joint with *8 mm* plate thickness inverse analysis

w_{PZ} [mm]	ε^*_{xx} [-]	z^*_{xx} [mm]	ε^*_{yy} [-]	z^*_{yy} [mm]	$\Delta\varepsilon^*_{yy}\, w_{pz}$ [mm]
18.5	-0.0048	0.602	-0.0170	1.166	0.171

By comparing the product of transversal strain range $\Delta\varepsilon^*_{yy}$ and width of plastic zone w_{pz} in Table 3 to Table 6, it is recognizable that the value represents the characteristic bending behaviour for this investigated joint. A value of *0.2 mm* matches the inherent deformation of the welded samples and the results of structural weld simulation.
To explore the applicability of the inverse analysis further on, a second T-joint with an increased plate thickness of *12 mm* was examined. The nominal throat thickness for this joint equals $a = 6\ mm$ and the corresponding net heat-input per unit length rises up to a value of $Q_{net} = 1{,}491\ J/mm$. Three-dimensional weld simulation depicted a transversal inherent deformation normal to the base plate of $u_z = 3.93\ mm$. The inverse analysis lead to an inherent deformation of $u_z = 3.42\ mm$, which matches the thermo-mechanical simulation. The remaining norm of residuals of *0.88 mm* is again caused by the randomly quantized values of the input parameters. Table 7 depicts the inherent strain values for the twelve millimetres joint. The product of transversal inherent strain range and width of plastic zone correlates to the numerically evaluated inherent deformation of the unclamped transversal joint.

Table 7 – Inherent strains for T-joint with *12 mm* plate thickness inverse analysis

w_{PZ} [mm]	ε^*_{xx} [-]	z^*_{xx} [mm]	ε^*_{yy} [-]	z^*_{yy} [mm]	$\Delta\varepsilon^*_{yy}\, w_{pz}$ [mm]
23.1	-0.0029	0.101	-0.0183	0.420	0.178

The similarity in angular distortion for both plate thicknesses can be correlated to the net heat-input per square plate thickness $Q\eta/h^2$. This related net heat-input has a value of $10.3\ J/mm^3$ for the twelve millimetre thick base plate and changes to $11.7\ J/mm^3$ for the transversal joint with a plate thickness of eight millimetres.

3.2 T-joint study

Several three-dimensional structural weld simulations were carried out to determine the characteristic inherent deformation behaviour. It has to be mentioned that the solid model has to possess a minimum welded length to reflect the distortion behaviour sufficiently. For short solid models, the geometry of the molten zone can not develop sufficiently and therefore the transversal bending of the joint is underestimated. The change in temperature at the start node of the weld path defines a characteristic value which can be related to the predicted distortion. Fig. 3.7a shows the course of the simulated normal displacement to the base plate after final cool-down. The corresponding transient temperature of the start path node at the time when the first weld run is finished is plotted on a second axis.

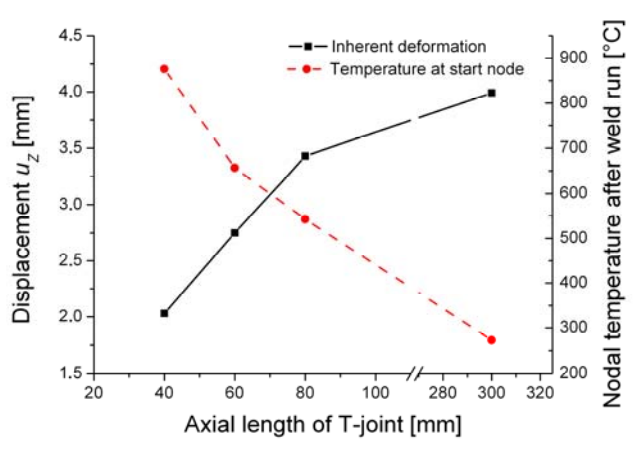

a) Influence of solid model length on distortion

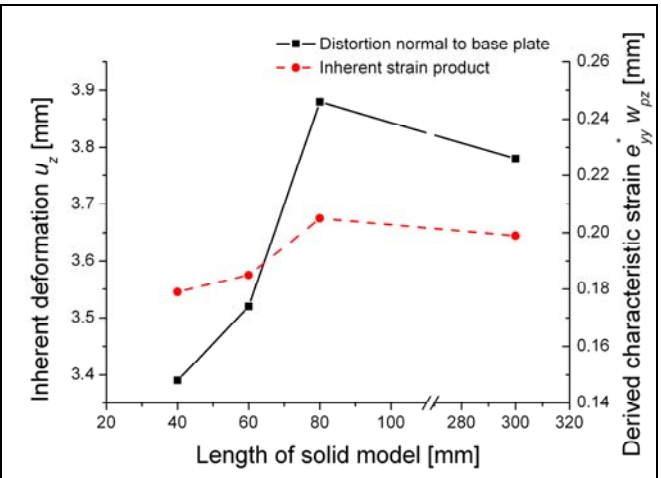

b) Adapted inherent strain results

Fig. 3.7 Influence of length of solid model on inherent deformation

Based on the transient change in temperature of the start node, an empirical correction function was generated which modifies the subsequent inherent strain evaluation. Fig. 3.7b depicts the inherent deformations based on corrected inherent strain values of solid models with different axial length. Although

the deformation varies up to half a millimetre, the mean value is in an improved agreement to the measurements. To get a proper plastic strain distribution for subsequent evaluation of the inherent strains for the simplified analysis, the length of the three-dimensional solid weld model should be at least five times the length of the molten zone.
Two-dimensional simulation results are not applicable for the unclamped condition of this thin-walled joint because of the missing three-dimensional axial supporting effect during cool-down of the weld seam. For comparison, the two-dimensional simulation leads to a deformation value of $u_z = 1.41\ mm$ which is quite lower than the measured distortion.

3.2.1 Influence of heat-input per unit-length

The effective throat thickness varies in the following investigations from two, four, up to seven millimetres. The plate thickness changes from eight up to twelve millimetres. Inherent strains were assessed both from the plastic strain distribution taken from thermo-mechanical simulation using *Sysweld*®, and by calculation with the analytical tool *Weldis*®. Fig. 3.8a depicts the change in transverse bending over the related net heat-input $Q\eta/h^2$. The distortion normal to the base plate increases linearly with the related heat-input, but for extreme heat-input values the behaviour is non-linear.

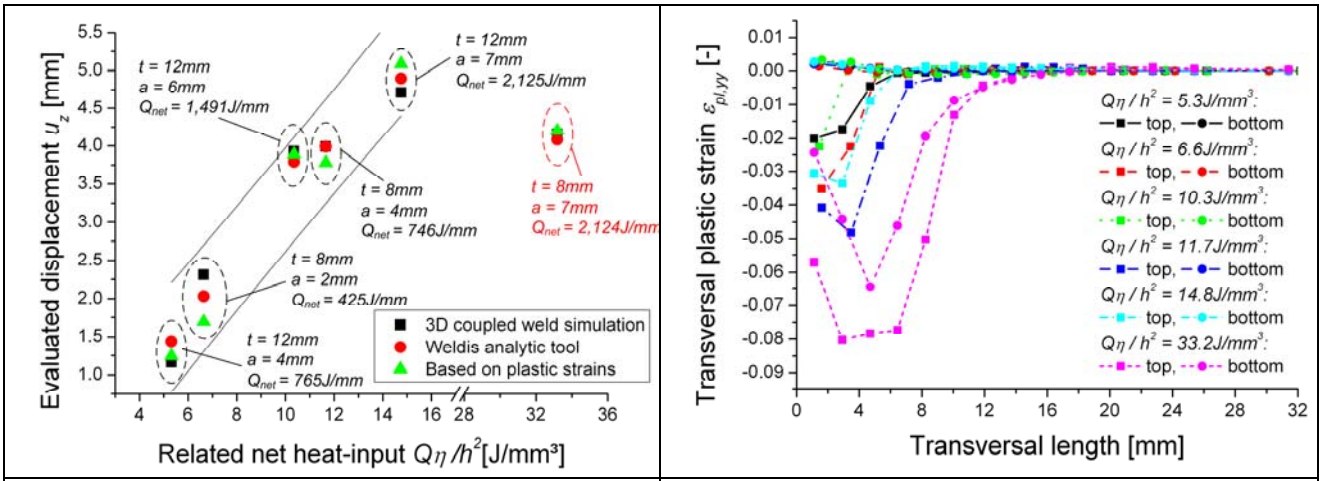

a) Effect of heat-input on distortion | **b) Transversal plastic strain distribution**

Fig. 3.8 Influence of heat-input per unit-length on inherent deformation

The course of the transversal plastic strain $\varepsilon_{pl,yy}$ at the top and bottom surface of the base plate is depicted in Fig. 3.8b. Basically, the distribution of the plastic strains at the top layer increases with the related net heat-input $Q\eta/h^2$. Similar tendencies were observed in [26] evaluating bead-on-plate joints.
For the uppermost numerically investigated related net heat-input of $33.2\ J/mm^3$, the plastic strain distribution at the bottom layer is also compressive. If this seam would be manufactured, the risk of a burn through the base plate is most presumable. The inherent deformation of the unclamped transversal joint is dominated by transversal bending. The difference in the plastic strain distribution between top and bottom layer of the base plate is characteristic, which is saturated for this case with extreme heat-input.

3.2.2 Effect of clamping condition

Clamping reduces the amount of inherent deformation significantly. In addition, the transient change in contact behaviour between base plate and padding support also influences the inherent deformation. If the base plate can move freely towards the ground, the distortion of the *8 mm* T-joint increases slightly from *3.99 mm* up to *4.15 mm*. Fig. 3.9a displays the change in distortion if the base-plates of the simulated transversal joints are clamped during the weld process and unclamped after final cool-down. For the additionally investigated transversal joints possessing a girth width of *730 mm*, the distortion value u_z is recalculated to a base plate girth width of *300 mm* for direct comparability of the results. The simulation models consider that the girth plate can not penetrate the padding support; in addition, the clamping condition at the lateral ends of the base plate fixes only the displacement normal to the base plate. The results of the inherent deformation based on plastic strain evaluation in Fig. 3.9a matches the three-dimensional thermo-mechanical coupled welding simulation quite well. On the other hand, the numerically calculated inherent deformation by *Weldis*® overestimates the distortion for short girth plate widths.

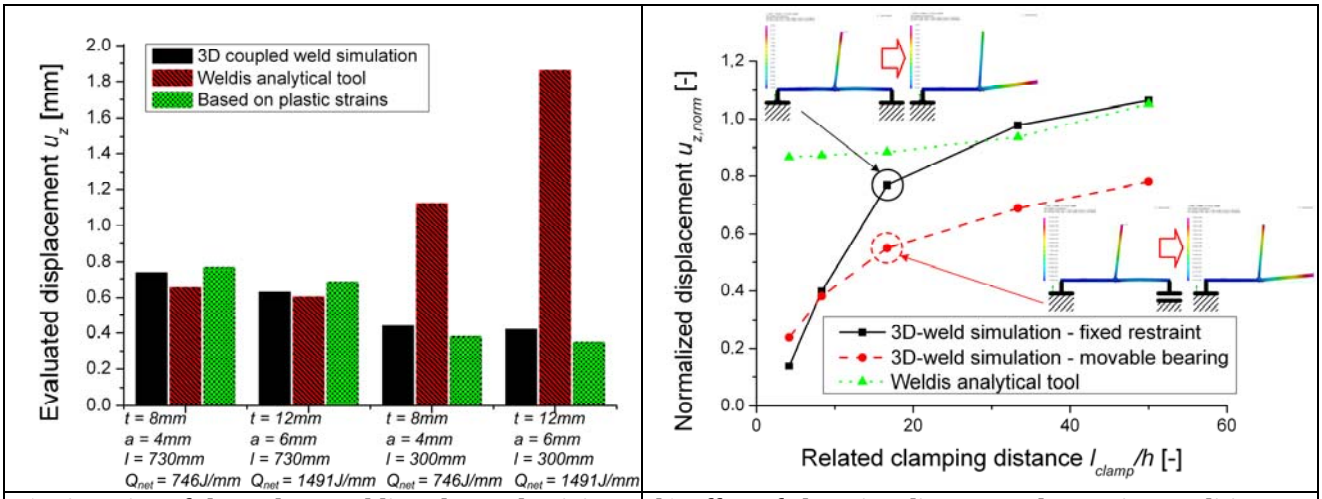

a) Distortion of throughout welding clamped T-joints | **b) Effect of clamping distance and restraint condition**

Fig. 3.9 Influence of clamping condition on inherent deformation

The results of a clamping distance study for transversal joints by three-dimensional elastic-plastic weld simulation are shown in Fig. 3.9b. The study was carried out for transversal joints with a base plate thickness of *12 mm* and a reduced throat thickness of *4 mm*. Such a cross-section is further on used in the investigations of an open-box corner stiffening frame. The related net heat-input exhibits a value of *5.3 J/mm*^{3}. The drawn results are normalized to support a better transferability to similar joint geometries. The displacement normal to the base plate u_z is plotted as unity value, whereat the maximal inherent deformation of $u_z = 1.73$ *mm* in the unclamped condition acts as reference value. The evaluated angular distortion depends strongly on the clamping distance and exploits to a potential law. The predicted inherent deformation in case of welding with a transversal movable bearing is about two thirds of the simulated distortion value if a fixed bearing on both girth plate ends is applied.

3.3 Corner stiffening frame

Beside the numerical investigations of the transversal joint, the applicability of the simplified inherent strain method is also examined for a corner stiffening frame. The geometry of the structure is shown in Fig. 3.10a. The frame consists of three steel plates, which are joined by six weld passes. After each pass, a certain intermediate cooling time is included. The overall weld sequence as well as heat-input per unit length and throat thickness are given in Fig. 3.10b. The structural elastic-plastic weld simulation starts with tacking of the plates whereat the three plates are fixed by the labelled constraints in Fig. 3.10a. After this procedure, the welding sequence of the plates starts with a transversal joint between base and corner plate. Afterwards, the web plate is joined with the base plate. Finally, the web plate is welded to the corner plate. The welded frame is unclamped after final cool-down at a time of *3,000s*. Base and corner plates possess a wall thickness of twelve millimetres, whereas the web plate is eight millimetres thick. The throat thicknesses and the subsequent heat-input values are similar to the previous transversal joint investigations.

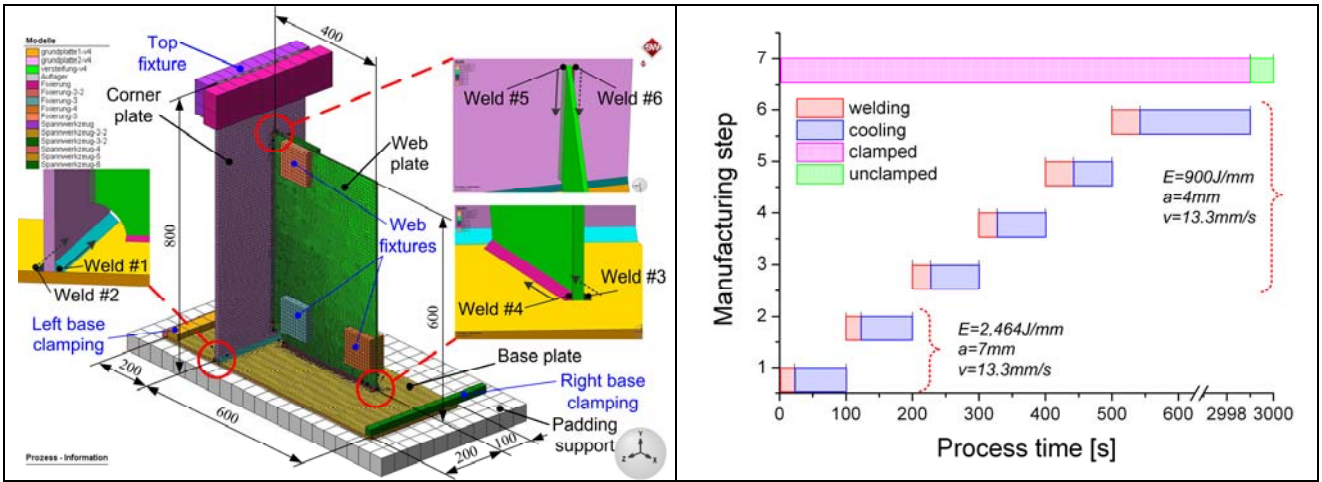

a) Geometry and general boundary conditions | **b) Weld sequence for numerical weld simulation**

Fig. 3.10 Corner stiffening frame model

The three-dimensional weld simulation of the corner stiffening frame was done using *simufact.welding*®. Different clamping conditions were examined to study the transferability of the thermo-mechanical coupled welding simulation to the simplified approach.

3.3.1 Model without base clamping

If the base plate is not clamped during the manufacturing process, the uppermost inherent deformation appears at the left side of the base plate, pointing in positive Y-direction. Fig. 3.11a depicts the distortion result of the solid model including a superimposed plot of the applied boundary conditions. The sketched deformed shape is scaled by a factor of ten to ensure better visibility of the distortion. Although no clamping condition is applied to the base plate, the contact between base plate and padding support avoids penetration of the base plate. Therefore, non-linear spring elements with high tension stiffness are applied to the nodes of the base plate in Fig. 3.11b to avoid penetration of the base plate into the fictive padding support in the simplified model. The stiff clamping conditions at the top of the corner plate and the web plate fixtures are modelled by boundary conditions of the corresponding nodes.

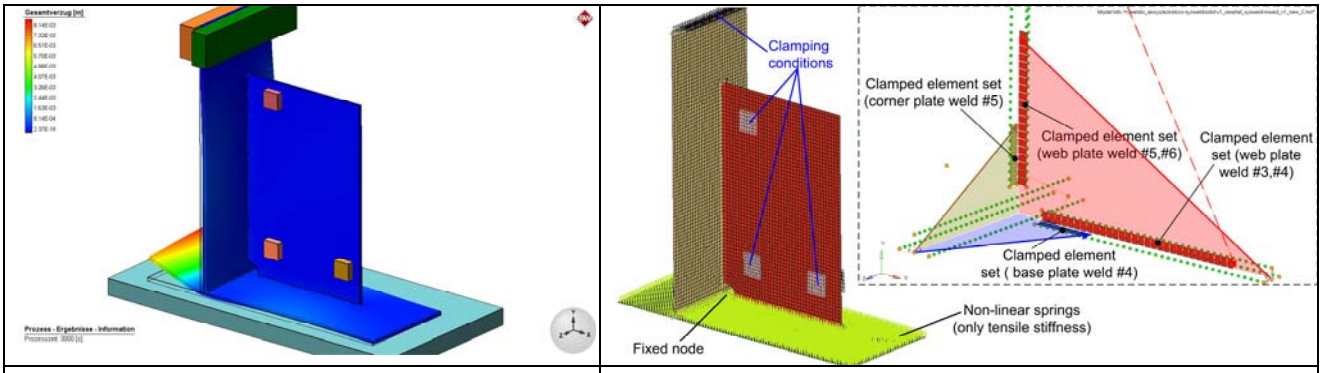

a) Three-dimensional weld simulation result | **b) Simplified shell model with inherent strain sets**

Fig. 3.11 Corner stiffening frame without base clamping conditions

Regarding the inherent strain distribution within the plastic width of each seam, the following procedure is suggested.

- Basically, the inherent strain values are constant for a specific seam dependent on the weld process parameters, local geometry, and clamping condition. To facilitate an improvement in distinguishing the plastic strain amount between clamped and unclamped condition, the length of each plastic zone is divided into two regions. The clamped region is mainly influenced from the neighboured plate edge. Hence, the clamped length of the seam is determined by drawing a line from the edge point covering an angle of thirty degrees. The covered patch is highlighted by a coloured triangle in Fig. 3.11b. The remaining elements outside the affected area are initialized with the inherent strain values for an unclamped joint geometry.
- The inherent strains are applied for each element set taking this specific ‘clamping’ condition into account. The orientation of the longitudinal and transversal direction should be determined by local material coordinate systems for each modelled joint. This facilitates independency from the global coordinate system.
- The influence of clamping and contact conditions can only considered in the simplified model in an approximated manner. As the padding support avoids the penetration of the base plate into negative Y-direction during welding and final cool-down, the simplified model maintains this behaviour approximately by use of contact elements or non-linear springs per affected node.

The amount of the inherent strain distribution and the width of the plastic zone are gained by evaluating the results of three-dimensional transversal joints simulation. In addition, the analytical tool *Weldis*® is used for the calculation of these values. The global coordinate system is identical for both the three-dimensional model and the numerical evaluation using the simplified inherent strain method. The shrinkage in positive Y-direction at the left corner of the base plate is calculated as $u_{Y,bp,left}$ = *7.4 mm* for the solid welding simulation, in case of the simplified method based on plastic strains, a distortion value of *6.0 mm*, and for *Weldis*® a significantly reduced value of *3.4 mm* are obtained. The simplified methods underestimate the angular distortion of the short overlap of the base plate, but the general deformation behaviour matches. The introduced initial strains lead to an elastic deformation of the simplified shell model, the accumulated strain energy of the model for this boundary condition has a value of *257 J*.

3.3.2 Production-oriented model

The corner stiffening frame is initially thoroughly clamped. The web plate is fixed with three welding jaws during tacking and immediately unclamped afterwards. The effect of tacking on distortion is therefore negligible. Both the base plate and the corner plate are clamped with fixed bearings at the ends. The frame is joined in accordance to the welding sequence depicted in Fig. 3.10b. After final cool-down, the clamping fixtures of the base and corner plate are released. This leads to the inherent deformation behaviour shown in Fig. 3.12a. The change in transient distortion during the weld process is evaluated for the corner of the flexible web plate and two edge points of the base plate. During welding of the six passes, no further change in clamping conditions occurs. Fig. 3.12b displays the charts of the transient change in distortion value for the three characteristic points. The maximum transient distortion is twice as large as the final inherent deformation. The counteracting effect of each T-joint pass is clearly recognizable. Welding of the fifth seam affects the evaluated lateral distortion of the web plate most. The effect of unclamping after final cool-down is insignificant for the base and corner plate, but recognizable in case of the more flexible web plate distortion.

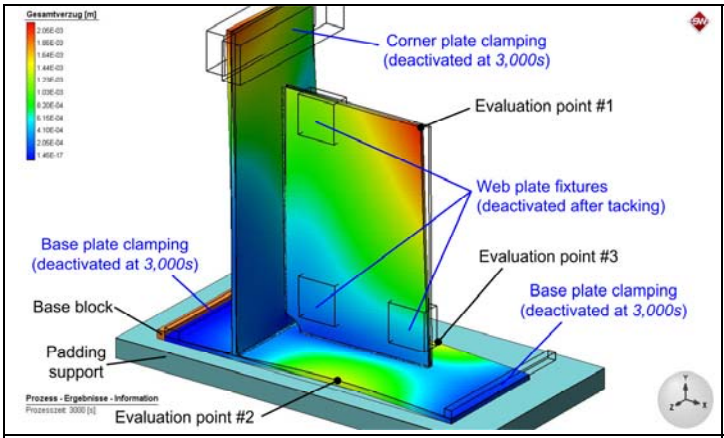

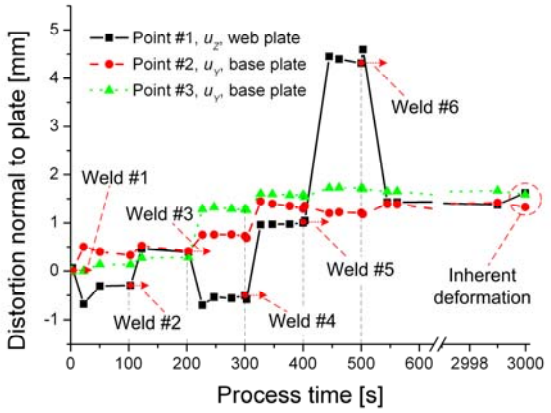

a) Three-dimensional weld simulation result and constraints | **b) Transient distortion at characteristic points**

Fig. 3.12 Corner stiffening frame with final unclamping – solid model

The inherent strain distribution of the simplified shell model is built-up in the proposed way; similar to that in Fig. 3.13a. The clamping of the base plate is considered in the simplified model by two constraint equations for the nodes of each base plate edge. The coupling of the displacements in Y-direction and rotations in Z-direction via constraint equations reflect the local inherent deformation of the base plate end regions which is only clamped during the weld process. The penetration of the base plate into the padding support is avoided by additional springs for each base plate node. The weak clamping condition at the top of the corner plate is considered by additional bidirectional springs. The plastic strains and the width of plastic zone of each seam were evaluated from short solid transversal joint models with adequate cross sections. In addition, inherent strains were calculated with the analytical tool *Weldis*®. The result of the elastic finite element calculation using inherent strains is shown in Fig. 3.14b. The distortion of the web plate is similar to the solid model, but at the base plate, deviations to the structural weld simulation are recognizable.

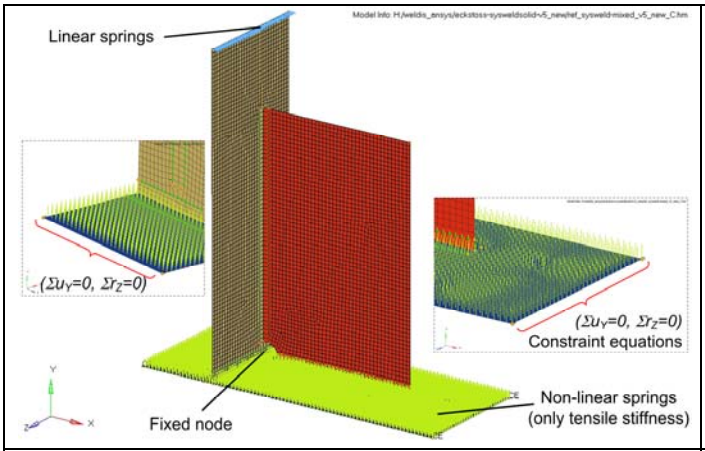

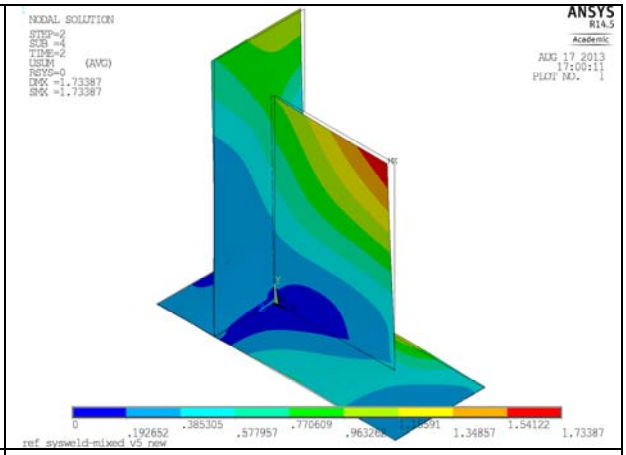

a) Simplified model with constraints | **b) Inherent deformation result**

Fig. 3.13 Corner stiffening frame with final unclamping – shell model

The result of the inherent deformation along six characteristic node paths is shown in Fig. 3.14. Each node path is evaluated normal to the corresponding plate plane. Node path #1 and #2 exploit that the shape of the inherent deformation along the base plate edge can be covered by the simplified method using the approximate boundary description with springs and constraint equations. Variances in the magnitude of the inherent displacement chart are unavoidable due to the simplifications in case of the elastic shell model. However, the location of the maximum distortion of the base plate is appropriately evaluated in the simplified model. The distortion of the web plate is analyzed along node path #3 and #4. The inherent deformation at the web plate corner node is predicted correctly. The evaluation of the distortion along node path #5 and #6 reveals that the inherent deformation is strongly influenced by the applied boundary definition at the top of the corner plate. The elastic property definition of the spring stiffness in the shell model has to approximately reflect the local plastic deformation behaviour of the clamped area during welding and cooling. Even so, the general distortion behaviour can be captured by the simplified conditions in the inherent strain model. The aggregated elastic strain energy of the shell model is about *202 J*, which indicates a smaller amount of general distortion. The clamping condition at the left side of the base plate leads to a significantly reduced amount in inherent transversal strain for the corresponding seam number two.

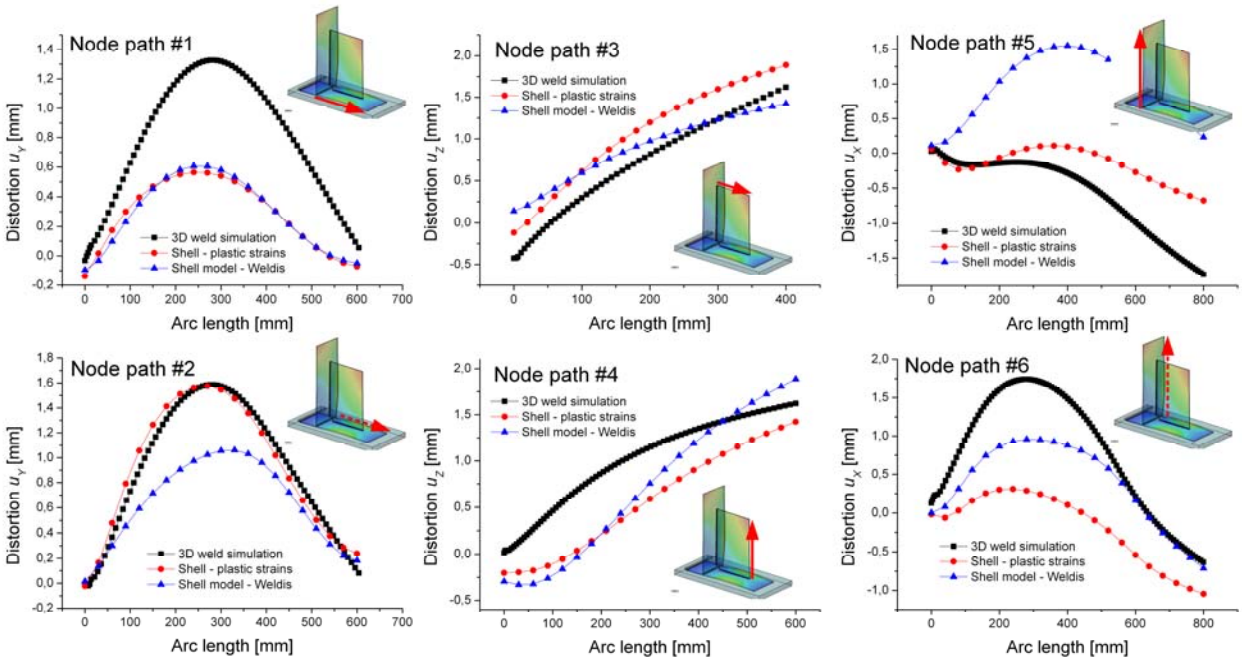

Fig. 3.14 Evaluation of distortion along characteristic node paths

The inherent strain method is capable of predicting the distortion of welded structures including interacting seams. Within one seam, the local stiffness of adjacent parts should be considered by distinguishing between different amounts of inherent strains for ‘free movable’ and ‘clamped’ joints. These inherent strains can be evaluated from transversal joints with appropriate cross-section geometry or by application of the analytical tool *Weldis*®. In the case of open-box or twisting sensitive welded steel frames, it is important to take the restraining conditions of the structure into account, especially if the structure is finally unclamped from the mounting device. Even if the prediction of the distortion after welding, cooling, and unclamping is not thoroughly accurate for the investigated open-box corner stiffening frame using the simplified method, the shape of the general deformation as well as the point of local maxima can be covered well within technical accuracy. For large scale structures, by including distortion sensitive non-linearities in contact or clamping conditions, a combination of the simplified inherent strain method applied to an elastic finite element shell model with a local elastic-plastic structural welding simulation might offer an interesting method to improve accuracy further on.

4 Conclusion

The inherent deformation of welded structures can be correctly predicted by three-dimensional structural weld simulation taking elastic-plastic material behaviour, metallurgical transformations, and contact conditions into account. The distortion of a transversal joint made of structural steel *S355* was simulated with the software packages *Sysweld*® and *simufact.welding*® and verified by experimental measurements.

The influence of heat-input per unit length and clamping conditions was studied for fillet welds with different plate thicknesses and base plate widths. The angular distortion of a transversal joint can be related to the net heat-input per unit length divided by the square of plate thickness. The effect of clamping length and clamping type has been examined for the T-joint exhibiting a power law for the influence of clamping distance. At a distance of ten times the plate thickness, the inherent deformation is about fifty percent of the unclamped distortion.

Based on these extensive three-dimensional weld simulation results, the inherent strains within the plastic zone were evaluated. These joint-specific values act as initial conditions in an elastic shell model, leading to a simplified prediction of the distortion. In addition, the inherent strain parameters were calculated with the analytical tool *Weldis*® for the examined joint geometries. The comparative investigations showed the basic applicability of the tool.

Finally, a method is depicted to map the inherent strains to more complex open-box and twisting sensitive models. An approximate procedure is presented for the investigated corner stiffening frame to cover the effect of welding induced elastic-plastic deformations in the contact and clamping areas by the use of non-linear springs or constraint equations in the linear inherent strain model. Although some deviations exist in the course of the inherent deformation charts, the general distortion behaviour and the position of local maxima can be assessed by the inherent strain approach within technically acceptable limits.

Acknowledgements

Financial support by the Austrian Federal Government (in particular from Bundesministerium für Verkehr, Innovation und Technologie and Bundesministerium für Wirtschaft, Familie und Jugend) represented by Österreichische Forschungsförderungsgesellschaft mbH and the Styrian and the Tyrolean Provincial Government, represented by Steirische Wirtschaftsförderungsgesellschaft mbH and Standortagentur Tirol, within the framework of the COMET Funding Programme is gratefully acknowledged.

Special thanks are to B. Jonsson, Volvo Construction Equipment, Sweden for the experimental work and A.A. Bhatti, Royal Institute of Technology, Division of Lightweight Structures, Sweden for discussion about simplified methods. Gratitude is expressed to P. Supancic, Research Institute for Advanced Technical Ceramics, Montanuniversität Leoben, Austria for granting permission for the academic usage of the software package *Ansys*® within this work.

References

[1] D. Deng, W. Liang, and H. Murakawa, “Determination of welding deformation in fillet-welded joint by means of numerical simulation and comparison with experimental measurements,” *Journal of Materials Processing Technology*, vol. 183, pp. 219 – 225, 2007.

[2] Y. H. Manurung, R. N. Lidam, M. R. Rahim, M. Y. Zakaria, M. R. Redza, M. S. Sulaiman, G. Tham, and S. K. Abas, “Welding distortion analysis of multipass joint combination with different sequences using 3D FEM and experiment,” *International Journal of Pressure Vessels and Piping*, 2013.

[3] M. S. Choobi, M. Haghpanahi, and M. Sedighi, “Effect of welding sequence and direction on angular ddistortion in butt-welded plates,” *Journal of Strain Analysis for Engineering Design*, vol. 47, no. 1, pp. 46–54, 2011.

[4] L.-E. Lindgren, “EnglishNumerical modelling of welding,” *EnglishComputer Methods in Applied Mechanics and Engineering*, vol. 195, no. 48-49, pp. 6710–6736, 2006.

[5] A. Barroso, J. Canas, R. Picon, F. Paris, C. Mendez, and I. Unanue, “Prediction of welding residual stresses and displacements by simplified models.

experimental validation," *Materials & Design*, vol. 31, no. 3, pp. 1338 – 1349, 2010.
[6] P. Mollicone, D. Camilleri, T. Gray, and T. Comlekci, "Simple thermo-elastic plastic models for welding distortion simulation," *Journal of Materials Processing Technology*, vol. 176, pp. 77 – 86, 2006.
[7] P. Mollicone, T. G. Gray, and D. Camilleri, "Experimental investigation and finite element analysis of welding induced residual stresses," *Journal of Strain Analysis for Engineering Design*, vol. 47, no. 3, pp. 140–152, 2012.
[8] D. Radaj, *Heat effects of welding*. Springer-Verlag GmbH, 1992.
[9] D. Camilleri and T. G. McPherson, "Procedural tacking fabrication influences on welding distortion," in *Proceedings of the International Conference on Advances in Welding Science & Technology for Construction, Energy & Transportation*, M. Kocak, Ed., 2010, pp. 403–408.
[10] K. Masubuchi, "Residual stresses and distortion in welds," in *Encyclopedia of Materials: Science and Technology (Second Edition)*, 2nd ed., K. H. J. Buschow, R. W. Cahn, M. C. Flemings, B. Ilschner, E. J. Kramer, S. Mahajan, and P. Veyssiere, Eds. Oxford: Elsevier, 2005, pp. 1 – 6.
[11] Z. Barsoum and A. Lundbäck, "Simplified FE welding simulation of fillet welds and 3d effects on the formation residual stresses," *Engineering Failure Analysis*, vol. 16, no. 7, pp. 2281 – 2289, 2009.
[12] C. Heinze, C. Schwenk, and M. Rethmeier, "Numerical calculation of residual stress development of multi-pass gas metal arc welding under high restraint conditions," *Materials & Design*, vol. 35, pp. 201 – 209, 2012.
[13] B. G. H. Jung and C. L. Tsai, "Fundamental studies on the effect of distortion control plans on angular distortion in fillet welded T-joints," *Weld Journal*, vol. 87, no. 7, pp. 213–223, 2004.
[14] T. Kannengiesser, T. Lausch, and A. Kromm, "Effects of heat control on the stress build-up during high-strength steel welding under defíned restraint conditions," *Welding in the World*, vol. 55, no. 07-08, pp. 58–65, 2011.
[15] Z. L. Zhang, Q. Y. Shi, Y. Y. Dongyang, Z. P. Cai, and D. C. Li, "Establishment and application of fixture constraint models in finite element analysis of welding process," *Acta Metallurgica Sinicia-Chinese Edition*, vol. 46, pp. 189–194, 2010.
[16] K. Satoh and Y. Ueda, "Japanese studies on structural restraint severity in relation to weld cracking (preliminary report)," *Welding in the World*, vol. 15, pp. 155–189, 1977.
[17] T. Schenk, I. Richardson, M. Kraska, and S. Ohnimus, "A study on the influence of clamping on welding distortion," *Computational Materials Science*, vol. 45, no. 4, pp. 999 – 1005, 2009.
[18] C. Heinze, C. Schwenk, and M. Rethmeier, "Influences of mesh density and transformation behaviour on the result quality of numerical calculation of welding induced distortion," *Simulation Modelling Practice and Theory*, vol. 19, no. 9, pp. 1847 – 1859, 2011.
[19] T. Schenk, I. Richardson, M. Kraska, and S. Ohnimus, "Modeling buckling distortion of DP600 overlap joints due to gas metal arc welding and the influence of the mesh density," *Computational Materials Science*, vol. 46, no. 4, pp. 977 – 986, 2009.
[20] D. Deng, "FEM prediction of welding residual stress and distortion in carbon steel considering phase transformation effects," *Materials & Design*, vol. 30, no. 2, pp. 359 – 366, 2009.
[21] D. Deng and H. Murakawa, "Influence of transformation induced plasticity on simulated results of welding residual stress in low temperature transformation steel," *Computational Materials Science*, vol. 78, pp. 55 – 62, 2013.
[22] H. Yunsok and S. R. Rajesh, "Thermal distortion analysis method for TMCP steel structures using shell element," in *Proceedings of the International Conference on Advances in Welding Science & Technology for Construction, Energy & Transportation*, M. Kocak, Ed., 2010, pp. 409–414.
[23] O. Muransky, C. Hamelin, M. Smith, P. Bendeich, and L. Edwards, "The effect of plasticity theory on predicted residual stress fields in numerical weld analyses," *Computational Materials Science*, vol. 54, pp. 125 – 134, 2012.
[24] M. Ottersböck, M. Stoschka, and M. Thaler, "Study of kinematic strain hardening law in transient welding simulation," *Mathematical Modelling of Weld Phenomena*, vol. 10, 2013, (in print).

[25] C. Heinze, C. Schwenk, and M. Rethmeier, “Effect of heat source configuration on the result quality of numerical calculation of welding-induced distortion,” *Simulation Modelling Practice and Theory*, vol. 20, no. 1, pp. 112 – 123, 2012.
[26] R. Wang, J. Zhang, H. Serizawa, and H. Murakawa, “Study of welding inherent deformations in thin plates based on finite element analysis using interactive substructure method,” *Materials & Design*, vol. 30, no. 9, pp. 3474 – 3481, 2009.
[27] Z. Zeng, L. Wang, P. Du, and X. Li, “Determination of welding stress and distortion in discontinuous welding by means of numerical simulation and comparison with experimental measurements,” *Computational Materials Science*, vol. 49, no. 3, pp. 535–543, Sep. 2010.
[28] J. Guirao, E. Rodriguez, A. Bayon, and L. Jones, “Use of a new methodology for prediction of weld distortion and residual stresses using FE simulation applied to ITER vacuum vessel manufacture,” *Fusion Engineering and Design*, vol. 84, no. 12, pp. 2187 – 2196, 2009.
[29] A. A. Bhatti and Z. Barsoum, “Development of efficient three-dimensional welding simulation approach for residual stress estimation in different welded joints,” *Journal of Strain Analysis for Engineering Design*, vol. 47, pp. 539–552, 2012.
[30] D. Deng and H. Murakawa, “Prediction of welding distortion and residual stress in a thin plate butt-welded joint,” *Computational Materials Science*, vol. 43, no. 2, pp. 353 – 365, 2008.
[31] D. Deng, H. Murakawa, and W. Liang, “Numerical simulation of welding distortion in large structures,” *Computer Methods in Applied Mechanics and Engineering*, vol. 196, no. 45, pp. 4613 – 4627, 2007.
[32] ——, “Prediction of welding distortion in a curved plate structure by means of elastic finite element method,” *Journal of Materials Processing Technology*, vol. 203, pp. 252 – 266, 2008.
[33] Y. Ueda, H. Murakawa, and N. Ma, “Chapter 2 - Introduction to measurement and prediction of residual stresses with the help of inherent strains,” in *Welding Deformation and Residual Stress Prevention*. Boston: Butterworth-Heinemann, 2012, pp. 35 – 53.
[34] H. Murakawa, D. Deng, N. Ma, and J. Wang, “Applications of inherent strain and interface element to simulation of welding deformation in thin plate structures,” *Computational Materials Science*, vol. 51, no. 1, pp. 43 – 52, 2012.
[35] J. Wang, M. Shibahara, X. Zhang, and H. Murakawa, “Investigation on twisting distortion of thin plate stiffened structure under welding,” *Journal of Materials Processing Technology*, vol. 212, no. 8, pp. 1705 – 1715, 2012.
[36] J. Wang, X. Yin, and H. Murakawa, “Experimental and computational analysis of residual buckling distortion of bead-on-plate welded joint,” *Journal of Materials Processing Technology*, vol. 213, no. 8, pp. 1447 – 1458, 2013.
[37] W. Liang and H. Murakawa, “An inverse analysis method to estimate inherent deformations in thin plate welded joints,” *Materials & Design*, vol. 40, pp. 190 – 198, 2012.
[38] T.-S. Jun and A. M. Korsunsky, “Evaluation of residual stresses and strains using the eigenstrain reconstruction method,” *International Journal of Solids and Structures*, vol. 47, no. 13, pp. 1678 – 1686, 2010.
[39] Y. P. Cao, N. Hu, J. Lu, J. Fukunaga, and Z. H. Yao, “An inverse approach for constructing the residual stress field induced by welding,” *Journal of Strain Analysis for Engineering Design*, vol. 37, no. 4, pp. 345–359, 2002.
[40] V. Michailov, N. Doynov, and C. Stapelfeld, “AiF Vorhaben IGF-Nr. 16673 BR Erweiterung eines analytisch-numerischen Hybridmodells für die Verzugssimulation von Großstrukturen,” Brandenburgische Technische Universität Cottbus, Tech. Rep., 2012.
[41] J. Goldak, A. Chakravarti, and M. Bibby, “A new finite element model for welding heat sources,” *Metallurgical Transactions B*, vol. 15, pp. 299–305, 1984.
[42] R. Singh, “Chapter 5 - Stresses, shrinkage and distortion in weldments,” in *Applied Welding Engineering*. Boston: Butterworth-Heinemann, 2012, pp. 175 – 190.